Small Structures

small structures

www.small-structures.com

RESEARCH ARTICLE OPEN ACCESS

Sub-50 nm Surface Nanopatterning via Nano-Seed-Assisted Stereolithography

Tae Wan Park[1,2] | Eun Bin Kang[1,3] | Young Lim Kang[1] | Yu Na Kim[1] | Yu Jin Kang[1] | Kang-Jun Baeg[4] | Hu Young Jeong[3] | Seung Sae Hong[5] | Sung-Dae Kim[1] | Min Sun Lee[6] | Diana Jeong[7] | Woon Ik Park[1,5,8]

[1]Department of Materials Science and Engineering, Pukyong National University (PKNU), Busan, Republic of Korea | [2]Querrey Simpson Institute for Bioelectronics, Northwestern University, Evanston, Illinois, USA | [3]Graduate School of Semiconductor Materials and Devices Engineering, Ulsan National Institute of Science and Technology (UNIST), Ulsan, Republic of Korea | [4]Department of Semiconductor Engineering, Pukyong National University (PKNU), Busan, Republic of Korea | [5]Department of Materials Science & Engineering, University of California, Davis, California, USA | [6]Department of Electrical Engineering & Computer Science, Daegu Gyeongbuk Institute of Science and Technology (DGIST), Daegu, Republic of Korea | [7]Department of Radiology, Stanford University, Stanford, California, USA | [8]RanoM R&D Center, RanoM Co., Ltd., Busan, Republic of Korea

Correspondence: Min Sun Lee (mslee1024@gmail.com) | Diana Jeong (jeongd@stanford.edu) | Woon Ik Park (thane0428@gmail.com)

Received: 9 March 2026 | **Revised:** 13 June 2026 | **Accepted:** 29 June 2026

Keywords: 3D printing | nanopatterning | nano-seed templates | stereolithography | sub-50 nm features

ABSTRACT

Three-dimensional (3D) printing based on stereolithography (SLA) enables microstructured objects, but sub-100 nm surface resolution remains difficult because of photopolymerization and resin diffusion. Here, we present a nano-seed-assisted SLA method for integrating sub-50 nm surface nanopatterns with 3D-printed structures. Si master molds with diverse nanoscale geometries are replicated into polymethyl methacrylate (PMMA) nano-seed templates, enabling controlled resin infiltration and high-fidelity pattern transfer from 250 nm to micrometer scales, including dots, holes, waves, and crosses. A conformal ultrathin inorganic barrier layer, such as platinum (Pt) or Ga_2O_3, suppresses resin-polymer intermixing, confines curing at the interface, and preserves pattern integrity. The method yields uniform sub-50 nm nanopatterns over chip-scale and larger areas up to 45 × 75 mm, verified by high-resolution TEM and elemental mapping. It integrates decorative or functional nanopatterns with complex 3D objects, exemplified by a 3D-printed Buddha sculpture. In addition to the hybrid assembly of separately prepared nanopatterned inserts, we further demonstrate the direct fabrication of a monolithic Buddha structure containing a localized nano-seed-derived patterned region, confirming that nanoscale surface ornamentation can be incorporated during the SLA printing process without requiring post-print assembly. Overall, nano-seed-assisted SLA offers a scalable route to high-resolution nanostructuring in 3D-printed materials.

1 | Introduction

Additive manufacturing (AM) significantly expands modern fabrication capabilities by enabling the construction of three-dimensional (3D) structures in a layer-by-layer manner [1–8]. This approach increases design flexibility and material diversity by allowing precise control over geometric form and composition that surpasses conventional subtractive or mold-based methods [9–11]. AM techniques directly convert digital models into physical structures and therefore support rapid and adaptable production of customized components used in lightweight mechanical systems [12, 13], biomedical scaffolds [14], metamaterials [15, 16], and photonic devices [17, 18]. The ability to generate architected features such as internal lattices or spatially graded structures further highlights the potential of AM for advanced material design [19–21]. Among AM platforms, stereolithography (SLA) receives

Tae Wan Park, Eun Bin Kang and Young Lim Kang contributed equally to this work.

particular attention because its light-driven photopolymerization process provides high surface smoothness and fine feature control [22–24]. The tight optical focus and predictable curing behavior of SLA make it suitable for fabricating microstructured features that require dimensional accuracy and smooth morphology, particularly when producing thin walls, high-aspect-ratio elements, or optically functional surfaces [25–28].

Despite these advantages, the practical resolution of SLA printing remains limited to the microscale range [29, 30]. The fundamental characteristics of optical diffraction, radical diffusion, and polymerization front broadening cause overcuring and spatial blurring that inhibit the formation of features smaller than 100 nm [31, 32]. These effects are especially problematic for shallow or densely packed patterns, where excess curing quickly leads to dimensional loss [33]. Additional process-dependent factors such as resin viscosity [34], exposure energy [35], and photoinitiator chemistry [36] further restrict nanoscale fidelity and often lead to rounded, widened, or merged features during high-resolution printing attempts. Creating nanoscale features directly at the resin surface of an SLA-printed object therefore remains a major unresolved challenge, particularly when attempting to form precise geometries such as narrow lines, sharp corners, or tightly curved nanoscale profiles [3, 37].

In contrast, top-down nanofabrication approaches including photolithography, electron-beam lithography, and nanoimprint lithography (NIL) provide precise control over sub-100 nm pattern geometries with excellent reproducibility [38, 39]. These techniques support a wide range of nanoscale motifs such as lines, dots, holes, gratings, and more complex periodic or quasiperiodic arrangements [40–42]. They are widely used in semiconductor devices, photonic crystals, sensors, and energy systems in which nanoscale placement accuracy controls functional performance [43–46]. Their process maturity enables high-resolution pattern transfer onto planar substrates over large areas and across diverse materials [47]. Although lithography-based techniques can generate highly precise nanoscale patterns and can be combined with additional transfer, molding, or etching processes to form 3D patterned topographies, their direct integration with freeform AM remains challenging. In particular, conventional lithographic and nanoimprint-based methods generally require predefined substrates, intimate contact with a patterning tool, or multiple sequential pattern-transfer steps. These requirements limit their straightforward use for incorporating nanoscale surface features into architecturally complex 3D-printed objects as an integrated part of the printing workflow. Therefore, a process that can introduce nanoscale surface patterns directly at the SLA printing interface would provide a complementary route for combining lithographic nanoscale precision with the geometric flexibility of AM.

To address this gap, this study introduces a nano-seed-assisted SLA framework that integrates nanoscale pattern replication into the SLA printing interface. Si master molds with various nanoscale geometries serve as templates and are replicated into polymethyl methacrylate (PMMA) nano-seed patterns that attach to the SLA build plate. These nano-seed templates guide resin infiltration during the curing process and support high-fidelity pattern transfer from 250 nm to several micrometers while accommodating diverse geometries such as dots, holes, waves, crosses, rings, linear gratings, and other complex motifs. A conformal ultrathin inorganic barrier layer made of materials such as platinum (Pt) or gallium oxide (Ga_2O_3) prevents intermixing at the resin and seed interface and enables precise nanoscale curing without pattern degradation. This system supports uniform replication of sub-50 nm nanopatterns, allows pattern formation across chip-scale and larger areas, and preserves feature fidelity without implying direct pattern formation on globally curved geometries. The approach also enables integration of symbolic or decorative nanopatterns with complex objects such as a 3D-printed Buddha. Importantly, beyond the post-print assembly of nanopatterned inserts onto selected regions, we demonstrate that a localized nano-patterned region can also be generated directly on a monolithic 3D-printed Buddha structure by initiating SLA growth from a Pt-coated PMMA nano-seed template. These results illustrate the practical applicability of the nano-seed strategy to geometrically intricate structures and its potential to enrich both functional and aesthetic aspects of 3D-printed materials.

2 | Results and Discussion

2.1 | Nano-Seed Concept and Interfacial Mechanisms for Nanoscale SLA Printing

The introduction of a nano-seed interface fundamentally transforms the SLA environment by establishing a lithographically defined contact layer that directs resin infiltration and localized photopolymerization. Figure 1a illustrates the overall configuration of the nano-seed-assisted SLA system in which a replicated PMMA pattern is attached to the build plate prior to immersion into a photocurable resin. A complete step-by-step fabrication workflow for PMMA nano-seed preparation and subsequent SLA integration is provided in the Supporting Information (Figure S1). During laser exposure from beneath the resin vat, light passes through the resin and interacts with the nanoscale topography present at the seed surface. The seed layer serves as the initial point of polymer network formation, and its geometric features act as nanoscale molds into which resin is drawn through capillary action. This process allows the earliest stages of photopolymerization to occur in a spatially confined environment, thereby circumventing the typical broadening of the curing front that limits resolution in conventional SLA.

Figure 1b highlights the critical role of the interfacial environment where the resin penetrates the nanoscale cavities of the PMMA seed prior to curing. Wetting behavior and capillary forces determine how efficiently resin fills these structures [48, 49]. The presence of an ultrathin Pt barrier layer enhances these effects by increasing surface energy and by promoting uniform resin spreading [50]. The Pt coating forms a conformal metallic skin that preserves the native geometry of the seed while serving multiple interfacial functions. By blocking radical diffusion and monomer penetration into the PMMA, the Pt barrier stabilizes the polymer seed against chemical degradation during exposure [51]. Rather than relying heavily on reflective effects, the Pt layer primarily contributes through diffusion blocking and surface-energy-mediated confinement, ensuring that photopolymerization remains localized [52]. These mechanisms

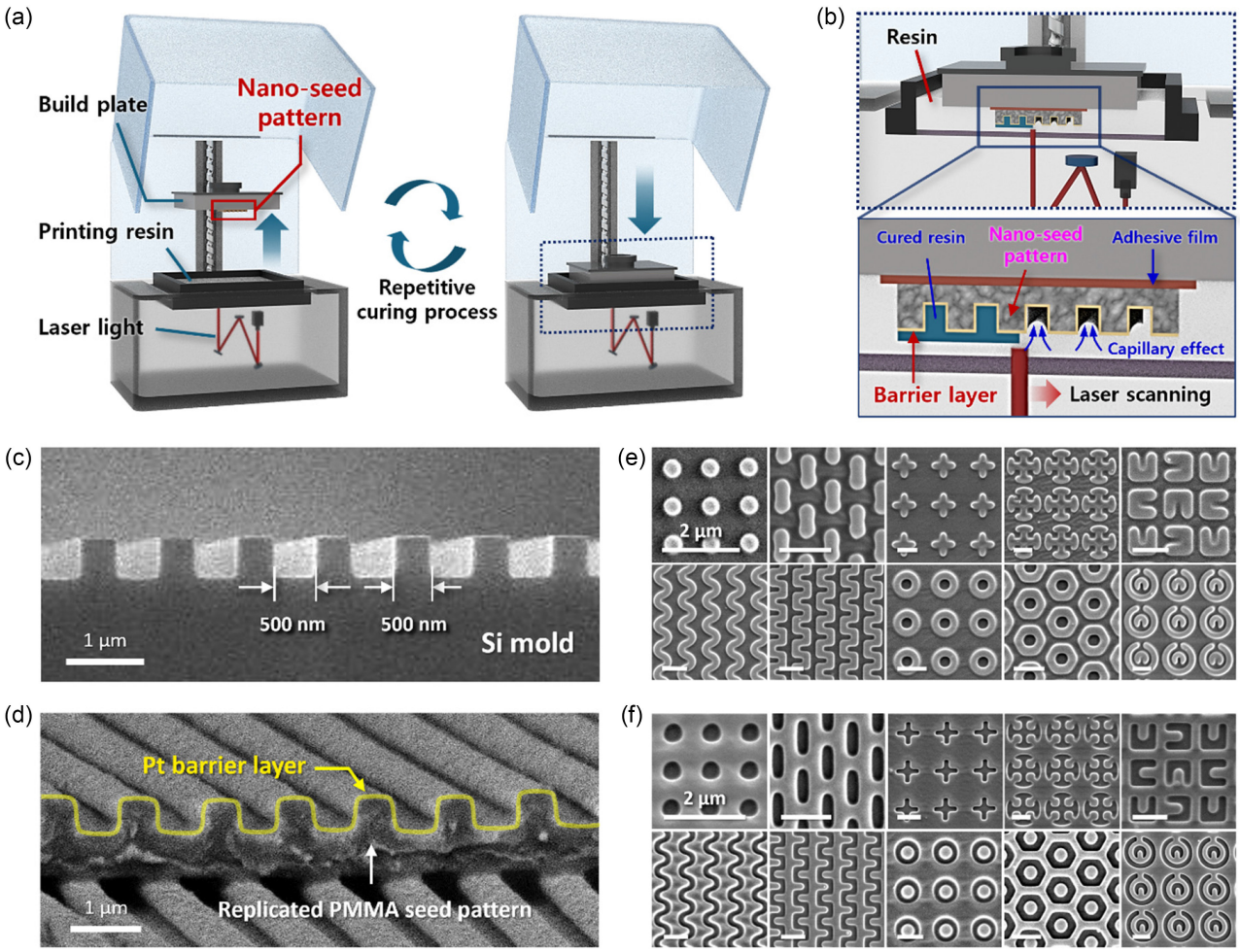

FIGURE 1 | Schematic illustration and fabrication of nano-seed templates for high-resolution stereolithographic 3D printing. (a) Overview of the nano-seed-assisted SLA process. A replicated PMMA nano-seed pattern fabricated from a Si master mold is attached to the build plate and immersed in a photocurable resin. During layer-by-layer laser exposure, the resin is selectively cured on the nano-seed surface, transferring nanoscale features onto the printed structure. (b) Enlarged view of the seed-resin interface showing nanoscale feature formation by capillary-driven resin infiltration and localized laser curing. An ultra-thin Pt barrier layer prevents resin intermixing and preserves feature fidelity. (c) SEM image of a Si master mold with 500-nm-wide line-and-space patterns. (d) Replicated PMMA nano-seed pattern transferred using spin-coated PMMA and PI film; the Pt layer ensures chemical isolation. (e) SEM images of various PMMA nano-seed patterns from Si molds, demonstrating versatility. (f) Corresponding inverse PMMA nano-seed structures confirming successful replication for nano-seed-assisted SLA.

collectively establish the nano-seed interface as a multifunctional scaffold capable of translating lithographic precision into an SLA environment.

The quality of the nano-seed itself is therefore central to this process. The seed templates are derived from Si master molds fabricated by KrF photolithography followed by reactive ion etching (RIE) to achieve submicron-scale periodicity. Additional Si master mold patterns used to construct the full sub-micron design library are presented in Figure S2, which illustrates the diversity of geometries replicated into the PMMA nano-seed templates. Figure 1c shows a Si master containing 500 nm line and space patterns with exceptional uniformity and smooth sidewalls. Additional Si master molds with finer resolutions are presented in Figure S3, which includes 50 nm line and space molds fabricated by ArF immersion lithography with double patterning as well as 250 nm molds produced by KrF photolithography. These masters also include a diverse library of motifs such as dots, holes, crosses, waves, and rings, all of which are faithfully transferred into PMMA through spin-coating and film detachment. Figure 1d presents a representative Pt-coated PMMA nano-seed pattern replicated from a Si master mold, confirming that the transferred structure maintains the full fidelity and nanoscale definition of the original template. Figure 1e,f show scanning electron microscope (SEM) images of Pt-coated PMMA nano-seeds replicated from Si masters with various nanoscale geometries, demonstrating that the replication process consistently reproduces diverse motifs while preserving coating uniformity and interfacial precision required for high-resolution SLA.

2.2 | Formation of Nanoscale Features During Nano-Seed-Assisted SLA

The performance of the nano-seed interface during SLA curing is evident in the cross-sectional structures shown in Figure 2a. When the build plate descends into the resin bath and the first laser scan is initiated, resin infiltrates the PMMA seed cavities

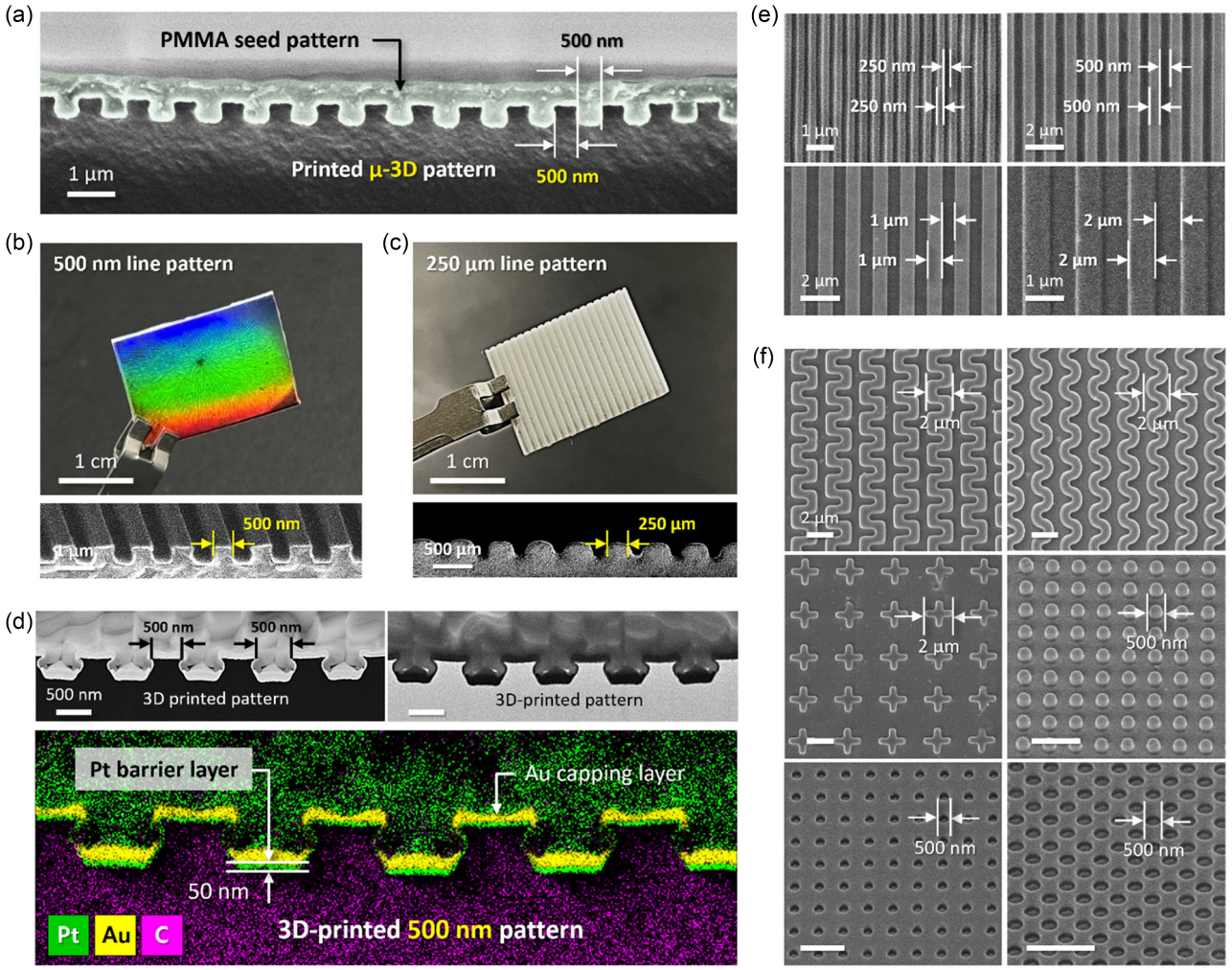

FIGURE 2 | High-resolution stereolithographic 3D printing using PMMA nano-seed templates. (a) Cross-sectional SEM image of a 3D-printed structure replicated from a 500 nm line PMMA seed pattern (seed not removed), showing resin infiltration by capillary action and the formation of a well-defined inverse pattern. (b) Chip-scale 500 nm line patterns (20 × 30 mm) show vivid structural coloration, and the optical image confirms this effect, while the cross-sectional SEM image verifies high-fidelity replication after dissolving the PMMA seed. (c) Finest pattern achievable with the same SLA printer without a nano-seed. A 250 μm line pattern exhibits severe rounding and poor definition, illustrating the intrinsic resolution limit of conventional SLA. (d) Bright-field and dark-field TEM images, together with EDS elemental maps (Pt, Au, C), demonstrating the integrity and key role of the ~30 nm Pt barrier layer in preventing intermixing between the PMMA seed and the resin during curing. (e) SEM images of printed line patterns with varying linewidths (250 nm, 500 nm, 1 μm, 2 μm), confirming scalable and high-fidelity pattern transfer. (f) SEM images of diverse nanopattern geometries including dot, hole, wave, and cross patterns, highlighting the geometric versatility of the nano-seed-assisted SLA approach.

through capillary-driven flow. The Pt surface significantly reduces the viscous resistance within these nanocavities by improving wetting behavior, thereby ensuring that the cavities are filled prior to the onset of curing. As the laser irradiates the resin, photoinitiated polymerization proceeds within these geometrically defined volumes. The confinement imposed by the seed structure prevents lateral broadening of the polymerization front, guiding the formation of a solid network that faithfully reproduces the shape of the cavity. The resulting printed feature is a precise inverse of the seed pattern, retaining sharp corners, smooth profiles, and consistent depths.

The impact of this interfacial constraint becomes even more apparent when the results are compared with conventional SLA printing. The commercial SLA printer used in this study was a Formlabs Form 3 system, which employs a 405 nm laser and a Light Processing Unit (LPU)-based optical system with a nominal laser spot size of approximately 85 μm. Therefore, the 500 nm line patterns obtained using the nano-seed interface are far smaller than the optical beam size of the printer and cannot be attributed to direct laser writing alone. As shown in Figure 2c, the finest structure that can be reproducibly fabricated without a nano-seed interface is a 250 μm-wide line for this specific SLA system, although higher-end SLA printers can achieve smaller features. The line exhibits blurred edges, rounded morphology, and significant dimensional deviation from the intended design. These deviations arise from radical diffusion, optical scattering, and the propagation of polymer chains beyond the illuminated region. Such effects are inherent to resin-based photopolymerization and cannot be eliminated through exposure adjustments alone. The intrinsic resolution limit of the commercial SLA printer used in this study was

independently evaluated, as shown in Figure S4, confirming a minimum reliably printable linewidth of approximately 250 μm. Consequently, standard SLA printing remains fundamentally limited to microscale resolution, regardless of the precision of the optical system. In contrast, Figures 2b and S5 demonstrate that the same printer equipped with a nano-seed interface can generate 500 nm line patterns across 20 × 30 mm areas with excellent uniformity and vivid structural coloration. This result indicates that the nano-seed-assisted SLA process decouples the lateral feature size from the laser spot size. In conventional SLA/DLP printing, the printed feature size is largely governed by the optical exposure profile, radical diffusion, optical scattering, and polymerization-front broadening. By contrast, in the nano-seed-assisted process, the laser primarily initiates photopolymerization, whereas the nanoscale lateral geometry is predefined by the lithographically patterned PMMA nano-seed cavities. Resin is drawn into these cavities through wetting and capillary filling, and curing proceeds within a geometrically confined resin volume at the seed/resin interface. Thus, the resolution-defining step is shifted from the optical domain to the physical and chemical domain of the template. This coloration may arise from optical interference due to the nanoscale periodicity, offering a rapid visual indicator of structural integrity. The cross-sectional SEM image confirms that the printed pattern matches the PMMA seed template with high fidelity. Additional pattern widths ranging from 250 nm to 2 μm, shown in Figure 2e, are also reproduced with consistent accuracy. These results validate the scalability of the approach across a wide range of nanoscale and microscale geometries.

Transmission electron microscopy (TEM) provides direct evidence of the interfacial processes responsible for this performance. Figure 2d shows bright-field and dark-field TEM images accompanied by elemental maps of Pt, Au, and C obtained through energy-dispersive X-ray spectroscopy (EDS). The Pt layer remains continuous after polymer curing and effectively separates the PMMA seed from the resin. No signs of chemical interdiffusion or physical damage are observed, confirming the stability of the barrier under SLA conditions. The Pt layer confines the polymerization zone primarily by serving as a physical and chemical barrier that suppresses resin penetration, monomer diffusion, and radical-mediated intermixing at the PMMA/resin interface, rather than through optical reflection. The successful pattern replication obtained using both metallic Pt and dielectric Ga_2O_3 barrier layers further indicates that continuous interfacial isolation, rather than a specific light-reflection effect, is the dominant requirement for nanoscale confinement. This interfacial isolation restricts photopolymerization to the resin adjacent to the seed surface, ensuring that nanoscale features are accurately reproduced without distortion. It is important to note that several metallic layers observed in the TEM and EDS analyses originate from the focused ion beam (FIB)-assisted lamella preparation rather than from the functional ultrathin barrier layers used during SLA printing. Specifically, the Au coatings, Pt capping layers, and carbon fillings applied during FIB milling serve only as protective or supportive layers for preparing TEM samples and should not be interpreted as part of the Pt or Ga_2O_3 barrier layers that govern nanoscale resin confinement during the nano-seed-assisted SLA process. The critical role of the Pt barrier layer is demonstrated in Figure S6, where the step-by-step results show that nanoscale features are preserved only when the PMMA nano-seed is coated with Pt, while the absence of the barrier leads to resin-PMMA intermixing and loss of pattern formation. The geometric versatility of the method is further demonstrated in Figure 2f, which shows dot arrays, hole lattices, wave patterns, and cross motifs. The replication of these complex layouts highlights the broad compatibility of the nano-seed approach with different nanoscale designs. The ability to reproduce such patterns under consistent but not necessarily identical printing conditions across all geometries underscores the reliability of the interfacial mechanism that governs resin infiltration and localized curing. These results establish nano-seed-assisted SLA as a robust and highly generalizable nanofabrication platform.

2.3 | Interfacial Engineering and Implications for Scalable Nanoscale Fabrication

The combined contributions of the PMMA seed and the Pt barrier enable SLA to surpass its intrinsic resolution limits. The seed provides a lithographically defined geometry that directs capillary flow and establishes a confinement region for photopolymerization. The Pt layer enhances wetting behavior, blocks diffusion, and restricts the spatial extent of the curing reaction. Together, these interfacial components define a nanoscale reaction chamber that converts the SLA system from a free-space polymerization process into a guided nanofabrication environment.

This interfacial engineering approach is mechanically robust and chemically stable, enabling reproducible pattern transfer across large areas. The results presented in Figures 1 and 2 establish a foundation for extending nanoscale patterning toward complex 3D-printed structures. Figures 3 and 4 further demonstrate the replication of sub-50 nm features, complex geometries including rings and dot-in-hole structures, and the integration of decorative or symbolic patterns with 3D-printed sculptures such as a Buddha figure. These demonstrations emphasize the potential of this technique to bridge the gap between high-resolution nanofabrication and the geometric freedom of AM.

2.4 | Expanded Nanopattern Diversity and Sub-50 nm Resolution Enabled by Nano-Seed-Assisted SLA

The nano-seed-assisted SLA framework significantly expands the range of nanoscale geometries achievable within resin-based AM while maintaining high interfacial control during curing. As shown in Figure 3a, complex motifs such as rings, nuts, and dot-in-hole arrangements are faithfully reproduced, demonstrating that the system can sustain tens-of-nanometers precision even for circular or nested shapes that are highly sensitive to overcuring effects. This versatility is further reflected in large-area dot-in-hexagonal-hole arrays (Figure 3b), which maintain consistent diameter, pitch, and symmetry across millimeter-scale regions despite the challenges associated with uniform capillary infiltration in dense nanoscale cavities. A corresponding 3D surface plot of the inset SEM image further highlights the uniform height profile and consistent topographical modulation within each hexagonal cavity, confirming that nanoscale infiltration remains spatially homogeneous across the array. The Pt barrier layer plays a decisive role in this uniformity by ensuring consistent

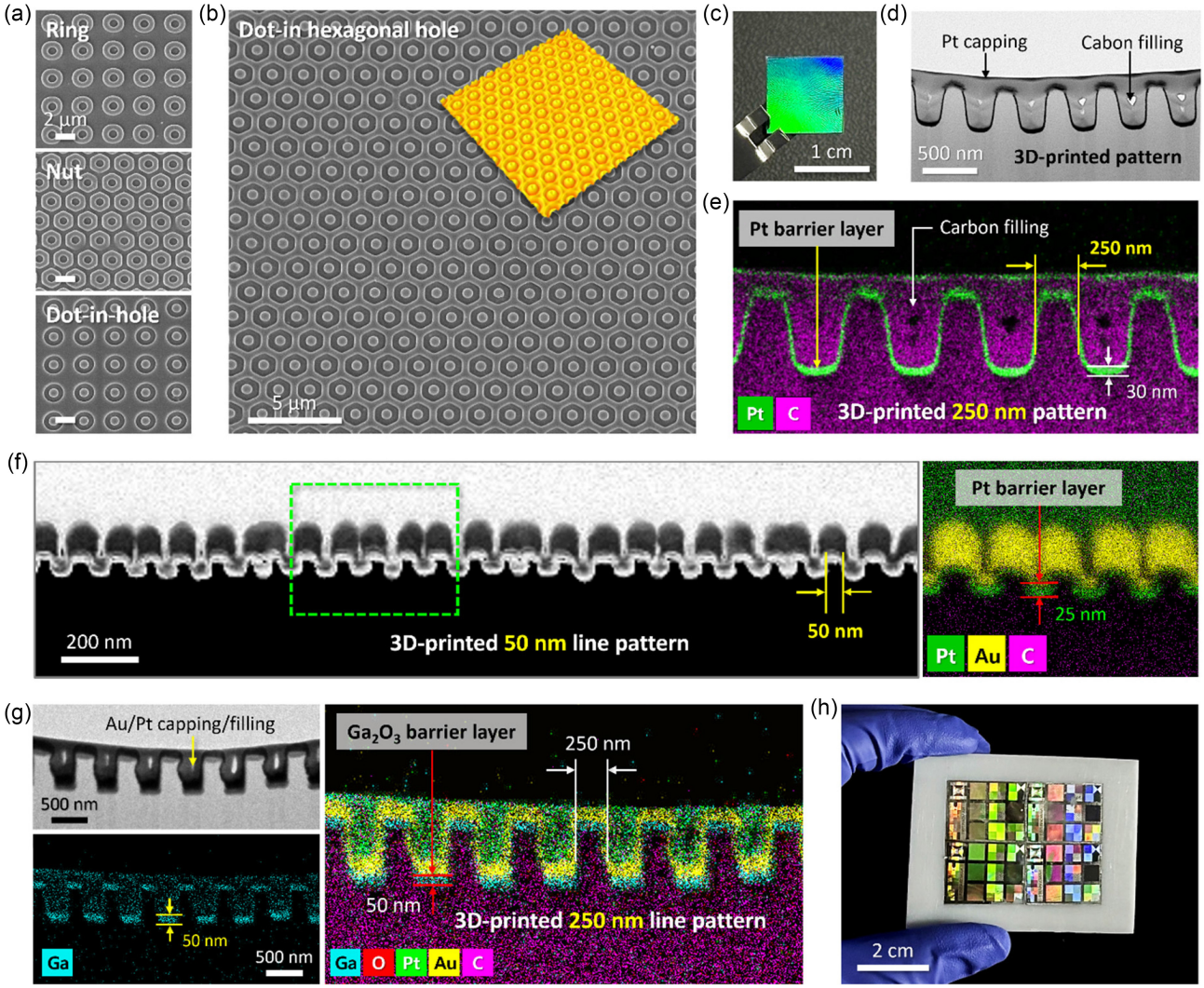

FIGURE 3 | High-fidelity replication of complex nanoscale geometries and sub-100 nm line patterns using the nano-seed-assisted SLA process. (a) SEM images of complex nanoscale geometries including ring, nut, and dot-in-hole motifs replicated from PMMA seed templates. (b) Large-area SEM image of dot-in-hexagonal-hole patterns, demonstrating uniform replication over extended regions. (c) Chip-scale 3D-printed structures (10 × 10 mm) containing 250-nm line patterns, showing reliable pattern formation across the entire area. (d) Bright-field TEM image of a 250-nm pattern, confirming well-defined feature formation and high pattern fidelity. (e) EDS elemental mapping (Pt, C) of the 250-nm structure, demonstrating the conformal coverage and critical role of the Pt barrier layer in preventing PMMA-resin intermixing during printing. (f) Sub-50 nm patterning enabled by nano-seed-assisted SLA. Bright-field TEM image (left) shows successful fabrication of a 50-nm line pattern; the magnified EDS map (right) reveals the Pt barrier layer and verifies its function in supporting nanoscale resin confinement. (g) 3D-printed 250-nm line pattern incorporating a Ga_2O_3 barrier layer. EDS mapping confirms uniform Ga_2O_3 coverage, demonstrating its role in suppressing resin diffusion and maintaining nanoscale structural fidelity. (h) Demonstration of chip-scale fabrication (50 × 30 mm) using nano-seed-assisted SLA, showing uniform nanostructures over a large printed area.

wetting behavior and preventing seed-resin intermixing, thereby enabling the fabrication of wafer-level nanostructures on 3D-printed components.

Chip-scale integration of 250 nm line patterns (Figure 3c) reveals vivid structural coloration, confirming periodic nanoscale ordering across 10 × 10 mm regions. Cross-sectional TEM imaging (Figure 3d) illustrates sharply defined profiles with uniform depth, and elemental mapping (Figure 3e) verifies the intact Pt barrier layer that preserves the PMMA-resin interface. These findings validate that the Pt layer confines photopolymerization to a defined nanoscale reaction zone. Remarkably, sub-50 nm line patterns (Figure 3f) also retain precise widths and sidewall definition; the Pt barrier layer maintains conformal nanometer-scale coverage and suppresses radical diffusion even at these limits. Moreover, the results obtained with the Ga_2O_3 barrier layer in Figure 3g show that diffusion suppression and pattern fidelity are not unique to Pt, indicating that the nano-seed-assisted SLA platform is broadly compatible with a variety of inorganic thin films and is inherently scalable. In addition to Pt and Ga_2O_3, a wide range of rigid inorganic thin films such as Al_2O_3, SiO_2, or TiO_2 may, in principle, serve as effective barrier layers, provided that they achieve conformal coverage and sufficiently suppress molecular interdiffusion at the seed-resin interface. This result confirms that the intrinsic limitation of SLA arises not from optical focusing but from the absence of spatial confinement at the reaction interface. The nano-seed platform provides such

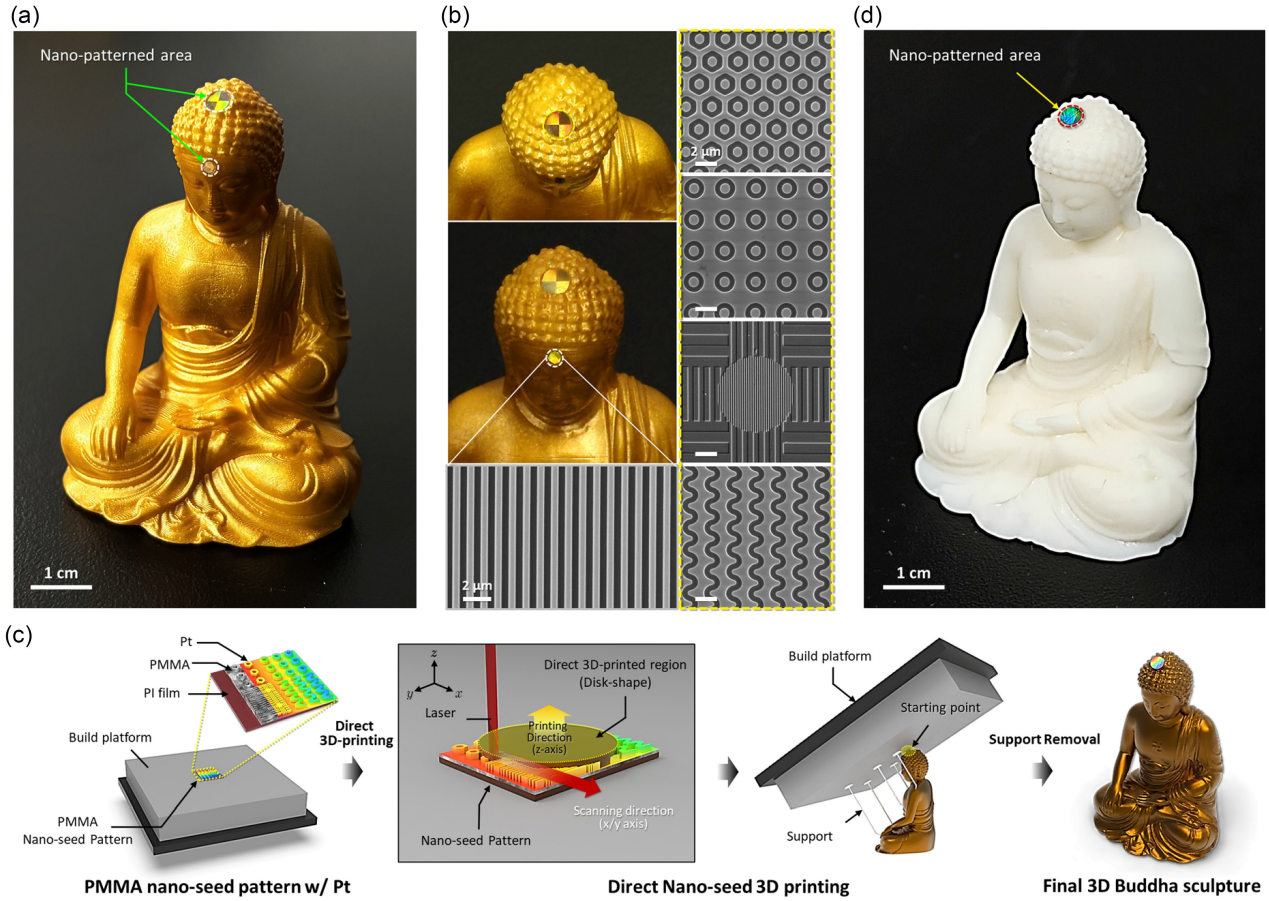

FIGURE 4 | Integration of decorative and symbolic nanostructures with 3D-printed Buddha sculptures via nano-seed-assisted SLA. (a) Photograph of the 3D-printed Buddha sculpture fabricated using the same SLA system, showing nano-patterned ornamentation integrated onto the forehead and head regions through post-print assembly of separately prepared patterned components. (b) Enlarged photographs and corresponding SEM images of the nano-patterned areas in the assembled Buddha structure. The head ornament incorporates four distinct nano-seed-derived patterns, while the forehead ornament features a 500 nm line pattern, demonstrating high-resolution nanopattern integration with a complex 3D object. (c) Schematic illustration of the direct nano-seed-assisted SLA printing process for fabricating a monolithic nano-patterned Buddha sculpture. A Pt-coated PMMA replica nano-seed was attached to the build platform, and printing was initiated from the disk-shaped head/forehead region containing the nano-seed pattern. Temporary support structures were included in the design to stabilize the tilted Buddha geometry during layer-by-layer printing and were removed after fabrication. (d) Photograph of the directly printed monolithic Buddha sculpture containing a localized nano-seed-derived patterned region on the head/forehead area without post-print assembly. The 3D model is adapted from "Gautama Buddha" by *fabonix* (CC BY 4.0).

confinement, enabling SLA to operate in a resolution regime previously inaccessible. Furthermore, while direct extrapolation must consider resin chemistry and interfacial physics, the demonstrated fidelity at 50 nm suggests that features approaching the 10 nm scale could become feasible if master molds and material parameters are optimized accordingly.

Figure 3h shows a representative nanopatterned area of 50 × 30 mm with minimal defects and high optical clarity, while the maximum nanopatterned area achieved in this study reaches 45 × 75 mm, as shown in Figure S7. These results confirm that nano-seed-based patterning remains compatible with the mechanical steps of SLA, including peeling, recoating, and repeated curing cycles, and that high-resolution nanopatterns can be integrated at early printing stages without compromising multilayer fabrication. Further scalability is supported by wafer-scale PMMA nano-seed patterns replicated from 8-inch Si molds using our thermally assisted nanotransfer printing (T-nTP) process (Figure S8), demonstrating that nano-seed preparation itself is not limited by substrate size. Because the nano-seed fabrication and SLA printing steps can be independently scaled by adjusting the seed area, barrier-layer deposition, and printer build volume, the accessible patterned region can be extended well beyond the areas demonstrated here. Although quantitative LER and CD uniformity analysis of the sub-50 nm polymeric features remains technically challenging because of electron-beam-induced damage and the need for FIB-based TEM preparation, the direct SEM and TEM observations confirm the formation of well-defined sub-50 nm patterns. In terms of scalability, the maximum patterned area is expected to be governed primarily by the size and uniformity of the replicated PMMA nano-seed, the available barrier-layer deposition area, the SLA build-platform size, and mechanical reliability during peeling, release, and seed removal, rather than by an intrinsic limitation of the nano-seed concept itself. Together, the results in Figure 3a–h establish nano-seed-assisted SLA as a robust and versatile nanofabrication route capable of achieving sub-50 nm resolution with large-area reproducibility.

2.5 | Nanoscale Ornamentation on Complex 3D Geometries

Selective integration of nanopatterns on designated regions is demonstrated in Figure S9, where only the PKNU letters were patterned through masked nano-seed deposition, resulting in localized structural coloration and nanoscale features. An additional advantage of the nano-seed approach is the ability to incorporate nanoscale ornamentation into architecturally complex 3D-printed objects. Figure 4a,b illustrate this concept using a Buddha sculpture in which nano-patterned inserts fabricated on planar substrates are subsequently mounted onto designated locations such as the forehead and head. The detailed fabrication route for this assembled Buddha structure is schematically shown in Figure S10. In this process, a PMMA nano-seed replica pattern supported by a PI film and coated with an ultrathin Pt layer was attached to the SLA build platform, and SLA printing was performed to form a disk-shaped photopolymer part containing the transferred nano-patterned surface. The printed nano-patterned disk was inserted into a recessed cavity predefined in the Buddha head, with its nano-patterned surface exposed at the target region, thereby demonstrating a hybrid strategy for selectively integrating nanoscale ornamentation into a conventionally printed macroscale 3D object. Because the nanopatterns are prepared on planar substrates before attachment, this result should be understood as a hybrid assembly strategy rather than direct nanoscale pattern formation on a globally curved surface. Nevertheless, the successful integration demonstrates the compatibility of nano-seed-derived nanostructures with complex geometries and the potential for combining high-resolution nanofabrication with large-format 3D printing. Magnified optical images and SEM results in Figure 4b show that four distinct nanopatterns are incorporated on the head region and a 500 nm line pattern is positioned at the forehead. Each pattern retains its structural fidelity after assembly, confirming that nano-seed-derived nanostructures maintain mechanical and dimensional stability when transferred from planar fabrication to curved 3D objects. This assembled Buddha structure therefore demonstrates a practical hybrid route for selectively placing nanoscale motifs onto complex printed components without disturbing the macroscopic SLA printing process.

To further address whether nano-seed-derived surface patterns can be incorporated without post-print assembly, we performed an additional direct-printing experiment using a Pt-coated PMMA replica nano-seed attached to the SLA build platform, as schematically described in Figure 4c. In this process, SLA printing was initiated from the disk-shaped nano-seed-patterned region corresponding to the head/forehead side of the Buddha model, while temporary support structures were included in the design to prevent tilting or collapse of the sculpture during layer-by-layer growth. After completion of the printing process, the supports were removed, yielding a monolithic Buddha structure containing a localized nano-seed-derived patterned region without attaching a separately fabricated patterned component. As shown in Figure 4d, the directly printed Buddha sculpture retains the overall 3D geometry and exhibits a localized patterned region on the head/forehead area. The nano-seed-assisted patterned region has a circular geometry with a diameter of approximately 3 mm and a thickness of approximately 2 mm, while the nanopatterned layer itself is approximately 350 nm thick. Although further optimization of the printing orientation, support design, and pattern-release process will be beneficial for improving yield and surface quality, this result clearly demonstrates the feasibility of directly fabricating an integrated 3D object containing nanoscale aesthetic surface features using the nano-seed-assisted SLA platform.

These hybrid and direct-printing demonstrations expand the design space for 3D-printed materials. Applications may include photonic surfaces whose optical response depends on geometric curvature, embedded anti-counterfeiting markers for secure manufacturing, and bioinspired textures that enhance adhesion or fluid interaction. Because the nanopatterns are produced through lithographically accurate nano-seeds and integrated with printed structures without substantial post-fabrication distortion, the technique allows the precision of semiconductor-grade nanofabrication to interface seamlessly with the geometric freedom of AM. An example of this concept is shown in Figure S11, where six nano-seed-patterned panels were assembled into a visually striking cubic structure and nanoscale patterns on the top, left, and right faces were confirmed by SEM imaging.

3 | Conclusions

This work demonstrates that nano-seed-assisted SLA provides a robust and scalable pathway for overcoming the intrinsic resolution limits of resin-based AM. By combining PMMA nano-seed templates with ultrathin inorganic barrier layers such as Pt or Ga_2O_3, the curing front can be spatially confined to the nanoscale, preventing diffusive overcuring and enabling the faithful replication of features well below 50 nm. The technique supports a wide diversity of geometries, including rings, nested hole structures, and subwavelength line patterns, while maintaining excellent uniformity across areas as large as 50×30 mm. Chip-scale structures exhibit sharp profiles and intact interfacial layers, confirming that the nano-seed platform reliably preserves structural fidelity during photopolymerization. Furthermore, the Buddha demonstrations show two complementary routes for incorporating nano-seed-derived surface features into architecturally complex 3D objects: post-print assembly of planar nanopatterned inserts and direct fabrication of a monolithic structure containing a localized nano-patterned region. The successful direct printing of the monolithic Buddha structure confirms that nanoscale surface ornamentation can be incorporated during the SLA process itself, although further optimization of support design, printing orientation, and pattern-release conditions will be important for improving process robustness. Collectively, these results illustrate that nano-seed-assisted SLA bridges nanoscale fabrication and macroscopic 3D printing, offering a versatile framework for producing high-resolution, multifunctional surfaces. Given the demonstrated precision at sub-50 nm dimensions, the approach is also expected to extend toward 10 nm-scale features with appropriate master molds, opening new opportunities for photonic engineering, anti-counterfeiting architectures, and advanced functional surface manufacturing.

4 | Methods

4.1 | Fabrication of Si Master Molds

Si master molds were fabricated using advanced photolithography combined with RIE to define nanoscale patterns with feature sizes ranging from 50 nm to several micrometers. Patterns with dimensions between 250 nm and 2 μm were produced by conventional KrF (248 nm) photolithography followed by CF_4/O_2-based RIE. For the 50 nm line patterns, ArF immersion lithography coupled with a double-patterning process was employed to achieve sub-100 nm periodicity with precise alignment control. After exposure and development, all samples underwent anisotropic dry etching to transfer the photoresist patterns into the Si substrate. The resulting Si masters exhibited smooth sidewalls and high aspect ratios suitable for subsequent replication. Each mold was cleaned sequentially in acetone, isopropanol, and deionized water, dried under nitrogen flow, and stored in a desiccator prior to PMMA replication.

4.2 | Replication of PMMA Nano-Seed Templates

Prior to polymer replication, the surface of the Si master mold was modified with a hydroxy terminated poly(dimethylsiloxane) (OH-PDMS) brush layer (5 kg mol^{-1}, 3 wt%) to facilitate clean detachment of the replicated film. The coating was applied by spin-coating the OH-PDMS solution onto the Si master, followed by thermal curing in a vacuum oven at 150 °C for 2 h to form a covalently bonded release layer. A PMMA solution (4 wt%, 100 kg mol^{-1}) dissolved in a mixed solvent of toluene: acetone: heptane = 4.5: 4.5: 1 by weight was then spin-coated onto the treated Si master at 5,000 rpm for 20 s to form a uniform thin film. After solvent evaporation, a polyimide (PI) adhesive film was laminated onto the PMMA-coated surface and gently peeled off, transferring the PMMA replica from the Si master to the PI support. The replicated PMMA nano-seed templates were subsequently mounted onto SLA build plates by applying a small amount of epoxy adhesive only to the backside of the seed plate. The active nano-patterned surface was located on the opposite side and was kept free from epoxy exposure. The epoxy was fully cured before resin immersion and served only to mechanically stabilize the nano-seed during resin immersion, laser exposure, and release, thereby minimizing possible interference with photocurable resin curing or nanoscale pattern replication.

4.3 | Deposition of Ultrathin Inorganic Barrier Layers

A conformal ultrathin metallic or oxide barrier layer was deposited onto the PMMA nano-seeds using an electron-beam (E-beam) evaporation system under a base pressure of 5×10^{-6} Torr. For Pt deposition, 4N (99.99%) Pt pellets were used as the source material, with a deposition rate of 0.1 Å s^{-1}, yielding a target thickness of typically 30 nm. Ga_2O_3 layers were deposited under similar vacuum conditions to comparable thicknesses. These barrier layers enhanced surface energy, suppressed monomer diffusion into the polymer substrate, and stabilized the seed-resin interface during photopolymerization.

4.4 | Nano-Seed-Assisted SLA Printing

SLA printing was conducted using a bottom-up 405 nm laser-based 3D printer equipped with a LPU-based optical system (Formlabs Form 3, laser power ≈250 mW, nominal laser spot size ≈85 μm) and a transparent resin vat. The Pt- or Ga_2O_3-coated PMMA nano-seed plate was mounted onto the build platform and immersed in a commercial photocurable resin (Formlabs White Resin V4). Each layer was printed with a nominal thickness of 25 μm, and the exposure energy was adjusted between 40 and 60 mJ cm^{-2} depending on the intended feature depth. During exposure, the laser-induced polymerization front propagated into the nanoscale cavities of the seed template via capillary-driven resin infiltration, enabling faithful transfer of nanoscale features onto the printed structure. Although Formlabs White Resin V4 was used as a representative commercial 405 nm photocurable SLA resin in this study, the nano-seed-assisted SLA process is expected to be extendable to other acrylate- or methacrylate-based SLA resins, provided that their wetting behavior, viscosity, curing kinetics, monomer functionality, and polymerization shrinkage are properly controlled. In particular, sufficient wetting and low-to-moderate viscosity are important for capillary filling of nanoscale seed cavities before gelation, whereas excessive viscosity, rapid gelation, or large volumetric shrinkage may lead to incomplete filling, pattern distortion, interfacial stress, or local delamination during curing and release. Therefore, when applying this method to other resin systems, exposure dose, layer thickness, resin viscosity, and barrier-layer surface chemistry may need to be optimized according to the resin formulation. After printing, uncured resin was removed by rinsing in isopropanol followed by gentle air drying.

4.5 | Characterization and Structural Analysis

Surface morphologies and nanoscale fidelity were analyzed using SEM (Thermo Fisher Quattro ESEM) operated at 10 kV. Cross-sectional structures were prepared by FIB milling (Thermo Fisher Helios 5 DualBeam) and examined by TEM (JEOL JEM-2100F) operated at 200 kV. EDS was conducted during TEM analysis to map the elemental distributions of Pt, Au, and C. Surface optical characteristics were evaluated using bright-field optical microscopy and spectroscopic reflectometry to investigate structural coloration effects arising from nanoscale periodicity.

Acknowledgments

T.W.P., E.B.K., and Y.L.K. contributed equally to this work. This work was mainly supported by the National Research Foundation of Korea (NRF) grant funded by the Korea government (MSIT) (RS-2025-02316993, No. RS-2024-00433654). This work was also supported by the NRF (RS-2023-00242507).

Funding

This study was supported by National Research Foundation of Korea (Grant RS-2025-02316993, RS-2024-00433654 and RS-2023-00242507).

Conflicts of Interest

The authors declare no conflicts of interest.

Data Availability Statement

The data that support the findings of this study are available from the corresponding author upon reasonable request.

References

1. S. H. Kim, Y. K. Yeon, J. M. Lee, et al., "Precisely Printable and Biocompatible Silk Fibroin Bioink for Digital Light Processing 3D Printing," *Nature Communications* 9 (2018): 1620.

2. F. Kotz, K. Arnold, W. Bauer, et al., "Three-Dimensional Printing of Transparent Fused Silica Glass," *Nature* 544 (2017): 337.

3. S. K. Saha, D. Wang, V. H. Nguyen, Y. Chang, J. S. Oakdale, and S.-C. Chen, "Scalable Submicrometer Additive Manufacturing," *Science* 366 (2019): 105.

4. A. Lee, A. Hudson, D. Shiwarski, et al., "3D Bioprinting of Collagen to Rebuild Components of the Human Heart," *Science* 365 (2019): 482.

5. D. Zhang, D. Qiu, M. A. Gibson, et al., "Additive Manufacturing of Ultrafine-Grained High-Strength Titanium Alloys," *Nature* 576 (2019): 91.

6. H. Yuk, B. Lu, S. Lin, et al., "3D Printing of Conducting Polymers," *Nature Communications* 11 (2020): 1604.

7. M. Park, J. Im, M. Shin, et al., "Highly Stretchable Electric Circuits from a Composite Material of Silver Nanoparticles and Elastomeric Fibres," *Nature Nanotechnology* 7 (2012): 803.

8. M. P. De Beer, H. L. Van Der Laan, M. A. Cole, R. J. Whelan, M. A. Burns, and T. F. Scott, "Rapid, Continuous Additive Manufacturing by Volumetric Polymerization Inhibition Patterning," *Science Advances* 5 (2019): eaau8723.

9. A. Sydney Gladman, E. A. Matsumoto, R. G. Nuzzo, L. Mahadevan, and J. A. Lewis, "Biomimetic 4D Printing," *Nature Materials* 15 (2016): 413.

10. C. Zhu, T. Y.-J. Han, E. B. Duoss, et al., "Highly Compressible 3D Periodic Graphene Aerogel Microlattices," *Nature Communications* 6 (2015): 6962.

11. R. D. Farahani, M. Dubé, and D. Therriault, "Three-Dimensional Printing of Multifunctional Nanocomposites: Manufacturing Techniques and Applications," *Advanced Materials* 28 (2016): 5794.

12. C. F. Dojan, M. Ziaee, A. Masoumipour, S. J. Radosevich, and M. Yourdkhani, "Additive Manufacturing of Carbon Fiber-Reinforced Thermoset Composites via in-Situ Thermal Curing," *Nature Communications* 16 (2025): 4691.

13. B. G. Compton and J. A. Lewis, "3D-Printing of Lightweight Cellular Composites," *Advanced Materials* 26 (2014): 5930.

14. S. Hong, D. Sycks, H. F. Chan, et al., "3D Printing of Highly Stretchable and Tough Hydrogels into Complex, Cellularized Structures," *Advanced Materials* 27 (2015): 4035.

15. S. Yuan, C. K. Chua, and K. Zhou, "3D-Printed Mechanical Metamaterials with High Energy Absorption," *Advanced Materials Technologies* 4 (2019): 1800419.

16. D. Chen and X. Zheng, "Multi-material Additive Manufacturing of Metamaterials with Giant, Tailorable Negative Poisson's Ratios," *Scientific Reports* 8 (2018): 1.

17. P.-I. Dietrich, M. Blaicher, I. Reuter, et al., "In Situ 3D Nanoprinting of Free-Form Coupling Elements for Hybrid Photonic Integration," *Nature Photonics* 12 (2018): 241.

18. A. Vyatskikh, R. C. Ng, B. Edwards, R. M. Briggs, and J. R. Greer, "Additive Manufacturing of High-Refractive-Index, Nanoarchitected Titanium Dioxide for 3D Dielectric Photonic Crystals," *Nano Letters* 20 (2020): 3513.

19. C. Crook, J. Bauer, A. Guell Izard, et al., "Plate-Nanolattices at the Theoretical Limit of Stiffness and Strength," *Nature Communications* 11 (2020): 1579.

20. X. Kuang, J. Wu, K. Chen, et al., "Grayscale Digital Light Processing 3D Printing for Highly Functionally Graded Materials," *Science Advances* 5 (2019): eaav5790.

21. H. K. Balakrishnan, L. F. Dumée, A. Merenda, et al., "3D Printing Functionally Graded Porous Materials for Simultaneous Fabrication of Dense and Porous Structures in Membrane-Integrated Fluidic Devices," *Small Structures* 4 (2023): 2200314.

22. X. Chen, W. Liu, B. Dong, et al., "High-Speed 3D Printing of Millimeter-Size Customized Aspheric Imaging Lenses with Sub 7 nm Surface Roughness," *Advanced Materials* 30 (2018): 1705683.

23. A. P. Kuo, N. Bhattacharjee, Y. S. Lee, K. Castro, Y. T. Kim, and A. Folch, "High-Precision Stereolithography of Biomicrofluidic Devices," *Advanced Materials Technologies* 4 (2019): 1800395.

24. S. Kawata, H.-B. Sun, T. Tanaka, and K. Takada, "Finer Features for Functional Microdevices," *Nature* 412 (2001): 697.

25. E. Behroodi, H. Latifi, and F. Najafi, "A Compact LED-Based Projection Microstereolithography for Producing 3D Microstructures," *Scientific Reports* 9 (2019): 19692.

26. X. Meng, S. Li, X. Shen, C. Tian, L. Mao, and H. Xie, "Programmable Spatial Magnetization Stereolithographic Printing of Biomimetic Soft Machines with Thin-Walled Structures," *Nature Communications* 15 (2024): 10442.

27. D. A. Walker, J. L. Hedrick, and C. A. Mirkin, "Rapid, Large-Volume, Thermally Controlled 3D Printing Using a Mobile Liquid Interface," *Science* 366 (2019): 360.

28. R. Su, J. Wen, Q. Su, et al., "3D Printed Self-Supporting Elastomeric Structures for Multifunctional Microfluidics," *Science Advances* 6 (2020): eabc9846.

29. Y. Sun, J. Cui, S. Feng, et al., "Projection Stereolithography 3D Printing High-Conductive Hydrogel for Flexible Passive Wireless Sensing," *Advanced Materials* 36 (2024): 2400103.

30. Y. Shan, J. Hua, and H. Mao, "3D Printing of Optical Lenses Assisted by Precision Spin Coating," *Advanced Functional Materials* 34 (2024): 2407165.

31. B. E. Kelly, I. Bhattacharya, H. Heidari, M. Shusteff, C. M. Spadaccini, and H. K. Taylor, "Volumetric Additive Manufacturing via Tomographic Reconstruction," *Science* 363 (2019): 1075.

32. T. A. Schaedler, A. J. Jacobsen, A. Torrents, et al., "Ultralight Metallic Microlattices," *Science* 334 (2011): 962.

33. M. S. Rill, C. Plet, M. Thiel, et al., "Photonic Metamaterials by Direct Laser Writing and Silver Chemical Vapour Deposition," *Nature Materials* 7 (2008): 543.

34. S. Xu, M. Fang, and X. Yan, "Research on Rheology and Formability of SiO_2 Ceramic Slurry Based on Additive Manufacturing Technology via a Light Curing Method," *ACS Omega* 7 (2022): 32754.

35. M. Zarek, M. Layani, I. Cooperstein, E. Sachyani, D. Cohn, and S. Magdassi, "3D Printing of Shape Memory Polymers for Flexible Electronic Devices," *Advanced Materials* 28 (2015): 4449.

36. D. Kam, O. Rulf, A. Reisinger, R. Lieberman, and S. Magdassi, "3D Printing by Stereolithography Using Thermal Initiators," *Nature Communications* 15 (2024): 2285.

37. M. Regehly, Y. Garmshausen, M. Reuter, et al., "Xolography for Linear Volumetric 3D Printing," *Nature* 588 (2020): 620.

38. T. W. Park, M. Byun, H. Jung, et al., "Thermally Assisted Nanotransfer Printing with Sub–20-Nm Resolution and 8-Inch Wafer Scalability," *Science Advances* 6 (2020): eabb6462.

39. W. I. Park, T. W. Park, Y. J. Choi, et al., "Extreme-Pressure Imprint Lithography for Heat and Ultraviolet-Free Direct Patterning of Rigid Nanoscale Features," *ACS Nano* 15 (2021): 10464.

40. C. Pina-Hernandez, A. Koshelev, S. Dhuey, et al., "Nanoimprinted High-Refractive Index Active Photonic Nanostructures Based on Quantum Dots for Visible Light," *Scientific Reports* 7 (2017): 17645.

41. D. Borah, S. Rasappa, M. Salaun, et al., "Soft Graphoepitaxy for Large Area Directed Self-Assembly of Polystyrene- *Block* -Poly(dimethylsiloxane) Block Copolymer on Nanopatterned POSS Substrates Fabricated by Nanoimprint Lithography," *Advanced Functional Materials* 25 (2015): 3425.

42. T. W. Park, Y. L. Kang, E. B. Kang, et al., "Direct Printing of Ultrathin Block Copolymer Film with Nano-in-Micro Pattern Structures," *Advanced Science* 10 (2023): 2303412.

43. M. J. Burek, Y. Chu, M. S. Liddy, et al., "High Quality-Factor Optical Nanocavities in Bulk Single-Crystal Diamond," *Nature Communications* 5 (2014): 5718.

44. D. Conteduca, I. Barth, G. Pitruzzello, C. P. Reardon, E. R. Martins, and T. F. Krauss, "Dielectric Nanohole Array Metasurface for High-Resolution Near-Field Sensing and Imaging," *Nature Communications* 12 (2021): 3293.

45. M. Jost, S. Albrecht, L. Kegelmann, et al., "Efficient Light Management by Textured Nanoimprinted Layers for Perovskite Solar Cells," *ACS Photonics* 4 (2017): 1232.

46. F. Schedin, A. K. Geim, S. V. Morozov, et al., "Detection of Individual Gas Molecules Adsorbed on Graphene," *Nature Materials* 6 (2007): 652.

47. V. Gupta, S. Sarkar, O. Aftenieva, et al., "Nanoimprint Lithography Facilitated Plasmonic-Photonic Coupling for Enhanced Photoconductivity and Photocatalysis," *Advanced Functional Materials* 31 (2021): 2105054.

48. T.-S. Wong, S. H. Kang, S. K. Tang, et al., "Bioinspired Self-Repairing Slippery Surfaces with Pressure-Stable Omniphobicity," *Nature* 477 (2011): 443.

49. Y. Zhang, Z. Dong, C. Li, et al., "Continuous 3D Printing from One Single Droplet," *Nature Communications* 11 (2020): 4685.

50. T. Kamegawa, Y. Shimizu, and H. Yamashita, "Superhydrophobic Surfaces with Photocatalytic Self-Cleaning Properties by Nanocomposite Coating of TiO_2 and Polytetrafluoroethylene," *Advanced Materials* 24 (2012): 3697.

51. T. K. Minton, B. Wu, J. Zhang, et al., "Protecting Polymers in Space with Atomic Layer Deposition Coatings," *ACS Applied Materials & Interfaces* 2 (2010): 2515.

52. A. A. Dameron, S. D. Davidson, B. B. Burton, P. F. Carcia, R. S. McLean, and S. M. George, "Gas Diffusion Barriers on Polymers Using Multilayers Fabricated by Al_2O_3 and Rapid SiO_2 Atomic Layer Deposition," *The Journal of Physical Chemistry C* 112 (2008): 4573.

Supporting Information

Additional supporting information can be found online in the Supporting Information section.